



Impact of particle characteristics on inferred emissions

S. M. Burrows et al.

Impact of modelled particle characteristics on emissions inferred by inversion of tracer transport

S. M. Burrows^{1,*}, P. J. Rayner², T. Butler^{1,**}, and M. G. Lawrence^{1,**}

¹Max Planck Institute for Chemistry, Mainz, Germany

²University of Melbourne, School of Earth Sciences, Melbourne, Australia

*now at: Pacific Northwest National Laboratory, Richland, Washington, USA

**now at: Institute for Advanced Sustainability Studies e.V., Potsdam, Germany

Received: 12 November 2012 – Accepted: 24 January 2013 – Published: 15 February 2013

Correspondence to: S. M. Burrows (susannah.burrows@pnnl.gov)

Published by Copernicus Publications on behalf of the European Geosciences Union.

Title Page

Abstract

Introduction

Conclusions

References

Tables

Figures



Back

Close

Full Screen / Esc

Printer-friendly Version

Interactive Discussion



Abstract

Model-simulated transport of atmospheric trace components can be combined with observed concentrations to obtain estimates of ground-based sources using various inversion techniques. These approaches have been applied in the past primarily to obtain source estimates for long-lived trace gases such as CO₂. We consider the application of similar techniques to source estimation for atmospheric aerosols, using as a case study the estimation of bacteria emissions from different ecosystem regions in the global atmospheric chemistry and climate model ECHAM5/MESy-Atmospheric Chemistry (EMAC).

Source estimation via Monte Carlo Markov Chain is applied to a suite of sensitivity simulations and the global mean emissions are estimated. We present an analysis of the uncertainties in the global mean emissions, and a partitioning of the uncertainties that are attributable to particle size, activity as cloud condensation nuclei (CCN), the ice nucleation scavenging ratios for mixed-phase and cold clouds, and measurement error.

Uncertainty due to CCN activity or to a 1 μm error in particle size is typically between 10 % and 40 % of the uncertainty due to observation uncertainty, as measured by the 5 %-ile to 95 %-ile range of the Monte Carlo ensemble. Uncertainty attributable to the ice nucleation scavenging ratio in mixed-phase clouds is as high as 10 % to 20 % of that attributable to observation uncertainty. Taken together, the four model parameters examined contribute about half as much to the uncertainty in the estimated emissions as do the observations. This was a surprisingly large contribution from model uncertainty in light of the substantial observation uncertainty, which ranges from 81 % to 870 % of the mean for each of ten ecosystems for this case study. The effects of these and other model parameters in contributing to the uncertainties in the transport of atmospheric aerosol particles should be treated explicitly and systematically in both forward and inverse modelling studies.

Impact of particle characteristics on inferred emissions

S. M. Burrows et al.

Title Page

Abstract

Introduction

Conclusions

References

Tables

Figures



Back

Close

Full Screen / Esc

Printer-friendly Version

Interactive Discussion



1 Introduction

Atmospheric aerosol particles are recognized as a critical part of the climate system, with their direct and indirect effects on climate identified as one of the key uncertainties in current understanding of climate change (Solomon et al., 2007). In order to advance prediction of aerosol climate impacts, their representation in global models must be improved, including their composition and distribution in the atmosphere. In particular, while much current research focuses on characterizing anthropogenic aerosols, naturally-occurring aerosols are still poorly characterized in global models, due to a variety of issues including sparsity of observational data, low model resolution, and inherent uncertainties in model parameterizations (Kinne et al., 2006; Huneus et al., 2011). While global models typically account for several classes of naturally-occurring aerosol (sea spray, dust) and man-made aerosol (sulfate, soot from industry and biomass burning), almost no global atmospheric model currently includes any explicit representation of primary biological aerosol particles (PBAP), material such as bacteria, pollen, fungal spores, and leaf fragments, despite the fact that these particles make up a large fraction of the observed aerosol at many locations (Jaenicke, 2005; Després et al., 2012).

While efforts to quantify emissions in models depend greatly on observations, these efforts can be classed into two broad groups: forward modelling and inverse modelling approaches. Briefly, forward-modelling approaches use empirical emissions data, derived e.g. from field experiments or industry data, and use ancillary information (e.g. maps, climate variables) to upscale to a global emissions map. In contrast, inverse modelling approaches use observed concentrations in conjunction with a model of atmospheric transport, and apply mathematical techniques to infer the necessary emissions required for the model to optimally match observations. Inverse problems typically are underconstrained, so their solution often requires the use of known emissions as a priori information in order to obtain a stable solution. In addition, the observed

ACPD

13, 4391–4432, 2013

Impact of particle characteristics on inferred emissions

S. M. Burrows et al.

Title Page

Abstract

Introduction

Conclusions

References

Tables

Figures



Back

Close

Full Screen / Esc

Printer-friendly Version

Interactive Discussion



variables typically differ from the modelled variables, e.g. in their spatial and temporal distribution and representativeness.

An inherent challenge of inverse modelling is the appropriate estimation of uncertainties, which can arise from many sources, including errors in the observational data, differences between model and observations in sampling location and representativeness, forecasting errors, and errors in modeling. This study considers some of the uncertainties inherent in the estimation of aerosol emissions by inversion. In particular, we examine the uncertainty contributed by the following model parameters: particle size, activity as cloud condensation nuclei (CCN), and the ice nucleation scavenging ratio. The uncertainty arising from these model parameters is compared to uncertainties arising from observations.

In this study, we use the estimation of bacteria emissions from different ecosystems as a case study. In Sect. 2, we briefly describe the observational data and the emissions model. In Sect. 3, we describe the model, including a discussion of key processes affecting aerosol removal, and the impact of selected model parameters on aerosol residence time. In Sect. 4, we briefly present the method used for inversion of atmospheric transport and estimation of sources, and present the main results from this inversion for different sensitivity cases. These results show how the estimated global mean emissions respond to changes in key model parameters. In Sect. 5, we introduce the term “normalized model uncertainties”, and present the normalized model uncertainties for a set of model parameters affecting atmospheric transport. In Sect. 6 we summarize and discuss key findings. In Appendix A, we describe in detail the numerical methods applied to calculate the inversion, and additional results are presented in Figs. A1–A4.

Impact of particle characteristics on inferred emissions

S. M. Burrows et al.

Title Page

Abstract

Introduction

Conclusions

References

Tables

Figures



Back

Close

Full Screen / Esc

Printer-friendly Version

Interactive Discussion



2 Bacteria concentration observations and emissions model

2.1 Observational basis

Published observations of bacteria concentrations in the atmosphere are scarce, and many suffer from methodological limitations. The concentrations of bacteria-containing particles in the atmosphere can be measured by a variety of methods with varying degrees of accuracy (Burrows et al., 2009b). Most commonly, atmospheric particulates are collected onto either a filter or an impaction plate, which is then analyzed for microbial content. One common method of analysis is the cultivation of bacterial cells on a culture medium, followed by counting of colonies. Because many bacteria are not readily cultivated, this method results in serious undercounting and a large uncertainty. A more robust, but also more labor-intensive method, is the use of microscopy, for instance optical microscopy combined with protein staining or the use of autofluorescence to identify microorganisms. Burrows et al. (2009b) reviewed a large number of published measurements of bacteria concentrations and recommended low, best and high estimates of the mean boundary-layer number concentrations of bacteria-containing particles in each of ten ecosystems, which are reproduced here in Table 1.

The high uncertainty in these estimates arises from uncertainties inherent in the observational methods discussed above, from the scarcity of observations, particularly long-term observations, and also from the high spatial and temporal variability in concentrations. The estimated uncertainty in the best-estimate mean concentrations derived from a review of the literature ranges from 81 % to 870 % of the mean for the ten individual ecosystems (Burrows et al., 2009a). Contrast this with an atmospheric component that can be measured far more precisely, such a CO₂, which due to its long atmospheric residence time has a much smaller degree of spatial and temporal variability, and the concentration of which can be measured with a high degree of precision, the relative uncertainty in each measurement being far less than 1 %.

Impact of particle characteristics on inferred emissions

S. M. Burrows et al.

Title Page

Abstract

Introduction

Conclusions

References

Tables

Figures



Back

Close

Full Screen / Esc

Printer-friendly Version

Interactive Discussion



2.2 Emissions model

Following Burrows et al. (2009a), bacteria tracers are emitted homogeneously from the ten lumped ecosystems presented in Table 1. The ecosystem classification is based on the Olson World Ecosystems data set (Olson, 1992), with ecosystems lumped into broader categories as described in Burrows et al. (2009a).

3 Global atmospheric model description, key processes and impacts of selected parameters

3.1 Description of global atmospheric model and simulations

All model simulations were conducted using a modified version of the global chemistry-climate model ECHAM5/MESy-Atmospheric Chemistry (EMAC), version 1.9. EMAC consists of a climate model that simulates the underlying meteorological parameters such as winds, combined with a number of submodels representing various physical and chemical processes in the atmosphere. The processes related to particulate emissions and loss processes are encapsulated in the submodels `ONLEM` (online emissions, Kerkweg et al., 2006b), `DRYDEP` (dry deposition onto land, water and plant surfaces, Kerkweg et al., 2006a), `SEDI` (sedimentation, Kerkweg et al., 2006a) and `SCAV` (precipitation scavenging, Tost et al., 2006). The submodel `CVTRANS` calculates particulate transport analogously to gas phase transport, as a sum of large-scale advection and parameterized small-scale convective transport (Tost et al., 2010; Lawrence and Rasch, 2005). The validity of the EMAC model for studies of large-scale aerosol transport and deposition has been established by comparison of simulated and observed deposition patterns of radioactive particles following the Chernobyl nuclear meltdown (Lelieveld et al., 2012).

Modifications to the model comprised updates to the `SCAV` submodel as described in Tost et al. (2010). All simulations were conducted at T63 horizontal resolution

Title Page

Abstract

Introduction

Conclusions

References

Tables

Figures



Back

Close

Full Screen / Esc

Printer-friendly Version

Interactive Discussion



Impact of particle characteristics on inferred emissions

S. M. Burrows et al.

Title Page

Abstract

Introduction

Conclusions

References

Tables

Figures

◀

▶

◀

▶

Back

Close

Full Screen / Esc

Printer-friendly Version

Interactive Discussion



($1.9^\circ \times 1.9^\circ$ or about 140×210 km at mid-latitudes) with 31 vertical levels up to 10 hPa, for five simulated yr (plus an additional year of spin-up). Initial meteorological fields were derived from the ECMWF ERA-15 reanalysis for 1 January 1990, following which, meteorology was simulated online. Monthly prescribed sea surface temperatures were applied from the AMIP-II data set (available from <http://www-pcmdi.llnl.gov/>).

Simulations were performed for monodisperse passive aerosol tracers, with aerodynamic diameters between $1 \mu\text{m}$ and $10 \mu\text{m}$, with and without CCN activity (CCN-ACTIVE: nearly all particles are activated as CCN in this size range; CCN-INACTIVE: no particles are activated as CCN). The removal processes active for each of the two particle types are summarized in Table 2. In the model setup used, cloud formation is independent of simulated aerosol concentrations, i.e. clouds affect aerosols (via wet removal), but aerosols do not affect clouds. The derived sensitivities thus refer only to the linear, one-directional effect of loss processes on concentrations, not to any potential nonlinear aerosol-cloud feedbacks.

3.2 Aerosol loss processes and their dependence on particle characteristics

Aerosols are removed from the atmosphere by both dry and wet deposition processes. For small particles, the most efficient removal is by coagulation with hydrometeors and dry surfaces associated with Brownian diffusion. For large particles, gravitational settling becomes increasingly efficient, and particles are more likely to be collected by hydrometeors via inertial impaction and interception, and subsequently removed via precipitation. For aerosol particles with aerodynamic diameters close to $1 \mu\text{m}$, precipitation scavenging is the dominant atmospheric loss process, but particles of this size fall into the so-called “scavenging gap” and thus have comparatively long atmospheric residence times (Pruppacher and Klett, 1997).

Particle size influences the rate of dry removal, and both particle size and chemical composition influence the rate of wet removal. In particular, particle chemical composition influences the likelihood that particles will act as heterogeneous nuclei for the formation of ice crystals and thus influences the likelihood of scavenging in mixed-phase

clouds; however, this is presently not accounted for in EMAC or most other global atmospheric models. Thus, uncertainties about particle characteristics also impact transport and loss processes (Pruppacher and Klett, 1997; Seinfeld and Pandis, 2006).

3.3 Ice nucleation scavenging and sensitivity cases

Ice nucleation scavenging in EMAC is calculated using a constant scavenging ratio. The ice and liquid water contents of clouds are each represented in EMAC by a single bulk variable. In the unmodified model (BASE case), ice nucleation is treated as follows. For mixed-phase clouds warmer than -35°C , the ice nucleation scavenging ratio is set to 0.1; otherwise it is set to 0.05. This ratio describes the fraction of the aerosol particles within the cloud that are incorporated into cloud ice crystals. The removal of these particles from a model grid box (by scavenging) further depends on the rate at which frozen precipitation falls from the grid box, relative to the amount of cloud ice within the grid box.

This parameterization is broadly consistent with field studies of aerosol partitioning in clouds at the Jungfraujoch (Swiss Alps; Henning et al., 2004; Verheggen et al., 2007), which show that the fraction of aerosol particles that are incorporated into the cloud liquid water and cloud ice decreases very rapidly at low temperatures and high ice mass fractions. This is likely due primarily to the Bergeron-Findeisen effect, which leads to the growth of a small number of ice crystals at the expense of the evaporation of a larger number of cloud droplets, which upon evaporation release the particles they contained back into the aerosol phase (Schwarzenböck et al., 2001). In those studies, the activated fraction ranges from 0.05 or less at temperatures below -15°C to about 0.7 at near-zero temperatures (Henning et al., 2004; Verheggen et al., 2007). The activated aerosol represents an upper limit on the aerosol that may be removed due to nucleation scavenging. Based on these results, we bound the ice nucleation scavenging parameter in the range 0.0–0.1 for “cold” clouds ($T < -35^{\circ}\text{C}$) and 0.1–0.7 for “mixed” clouds ($-35^{\circ}\text{C} \leq T \leq 0^{\circ}\text{C}$).

Impact of particle characteristics on inferred emissions

S. M. Burrows et al.

Title Page

Abstract

Introduction

Conclusions

References

Tables

Figures

◀

▶

◀

▶

Back

Close

Full Screen / Esc

Printer-friendly Version

Interactive Discussion



Impact of particle characteristics on inferred emissions

S. M. Burrows et al.

Title Page

Abstract

Introduction

Conclusions

References

Tables

Figures

◀

▶

◀

▶

Back

Close

Full Screen / Esc

Printer-friendly Version

Interactive Discussion



Four sensitivity cases were tested, in addition to the BASE case (Table 3). In the cases SENS_COLD and SENS_MIXED, small perturbations were made to test the quasi-linear response of the model to a 1 % change in the respective parameter. The SENS_MIXED case resulted in an appreciable perturbation of aerosol concentrations in the mid-latitude tropopause region and the surface atmosphere at high-latitudes (not shown). However, the effect on estimated emissions was too small to be detected within the random noise of the Monte Carlo simulation. These cases will not be discussed in further detail, but are included in some of the presented results.

In the cases LIM_COLD and LIM_MIXED, we used larger perturbations in order to gauge the response of the Monte Carlo emissions estimate to a larger perturbation to the respective ice scavenging coefficients, respectively changing the coefficient for cold clouds from 0.05 to 0.1, and the coefficient for warm clouds from 0.1 to 0.7.

3.4 Impact of size and emission region on particle residence times

The global mean atmospheric residence times of particles depend strongly on whether they act as CCN, on the particle diameter, and on the region from which they are emitted (Fig. 1). Atmospheric residence times are longest for particles emitted from deserts, where there is little scavenging and dry convection rapidly transports particles to high altitudes. Residence times of 1 μm particles are shortest for particles emitted from oceans, where scavenging is strongest. For larger particles and CCN-INACTIVE particles, for which particle lifetime is more strongly driven by dry deposition processes, particle lifetimes are shortest in crops and forest regions, where plants increase friction and provide large surfaces for deposition. The effect of particle size on residence time is somewhat stronger for CCN-INACTIVE particles than for CCN-ACTIVE particles, since the residence time for CCN-INACTIVE particles is more strongly determined by dry deposition.

4 Source inversion by Monte Carlo methods

4.1 Overview

In this section, we invert the atmospheric transport problem and estimate sources from information about concentrations. We describe the methods used in Sect. 4.2, and a more detailed description can be found in Appendix A1 and standard texts (e.g. Tarantola, 2005). We present and discuss the results of the inversion in Sect. 4.3.

4.2 Inversion method

4.2.1 Forward model, model parameters and data vector

The forward model is described by the following elements:

1. The observable quantities \mathbf{d} : a vector representing the mean concentration of bacteria in each ecosystem.
2. The model (parameters) \mathbf{m} : a vector representing the surface fluxes in each ecosystem.
3. The model function $\mathbf{m} \mapsto g(\mathbf{m})$: The results from global atmospheric model simulations (as described in Sect. 3) are used to derive a simplified statistical model of inter-ecosystem transport. The modelled concentrations are linear in source strengths so the model can be represented by a 10×10 matrix describing the relationship between homogeneous, constant emissions from each source ecosystem and mean boundary-layer concentrations in each destination ecosystem. The simulated concentrations are given by the product of the inter-ecosystem transfer matrix \mathbf{G} and the flux vector \mathbf{m} :

$$g(\mathbf{m}) = \mathbf{G}\mathbf{m}. \quad (1)$$

The linearity of g is guaranteed by design in the EMAC model setup used here (neglecting small numerical errors), as all simulated removal rates are proportional to aerosol mixing ratios, and there is no feedback of aerosol concentrations onto other model variables such as cloud microphysics or meteorological variables.

4.2.2 Observable parameters

For the observations we assume Gaussian uncertainty, with coefficients taken from Table 1: the mean value is given by the best-estimate, and the standard deviation is given by one-quarter of the range of concentration estimates for the respective ecosystem, i.e. (high estimate – low estimate)/4. We assume no prior information about the value of d .

4.2.3 Model prior and model error

We tested the effects of a prior positivity constraint on the model, i.e. a constraint that disallows negative emissions. Inversions with this constraint are designated PRIOR-POS, and the model prior $\rho_M(\mathbf{m})$ is given by:

$$\rho_M(\mathbf{m}) = \begin{cases} \mu_M(\mathbf{m}), & \mathbf{m} \geq 0 \\ 0, & \mathbf{m} < 0 \end{cases} \quad (2)$$

where $\mu_M(\mathbf{m})$ represents the homogeneous probability distribution for model parameters (Tarantola, 2005, Ch. 1). A positivity constraint can be justified by assuming that the atmospheric model accurately represents the removal of aerosols from the atmosphere, or at least does not underestimate removal. However, this constraint may not be justified if the atmospheric model underestimates removal. For this reason, and to illustrate the effect of the prior positivity constraint, we also present some results from inversions for which no prior constraint is applied, designated NO-PRIOR:

$$\rho_M(\mathbf{m}) = \mu_M(\mathbf{m}) \quad (3)$$

Impact of particle characteristics on inferred emissions

S. M. Burrows et al.

Title Page

Abstract

Introduction

Conclusions

References

Tables

Figures

◀

▶

◀

▶

Back

Close

Full Screen / Esc

Printer-friendly Version

Interactive Discussion



For the purposes of the inversion, we do not explicitly include the model error. (Taranola, 2005, Eq. 1.74) shows that, for Gaussian error statistics one can add the variances associated with model error and observational error. Given the very large observational errors we treat the model error as negligible. In other words, each realization of the model function $g(\mathbf{m}) = \mathbf{G}\mathbf{m}$ is taken to exactly describe the behavior of the global atmospheric model in the respective configuration.

4.2.4 Likelihood function

The likelihood function $L(\mathbf{m})$ is a measure of how well the model \mathbf{m} explains the observations:

$$L(\mathbf{m}) = \int_{\mathbf{D}} d\mathbf{d} \theta(\mathbf{d}|\mathbf{m}) = \prod_{i=1}^N \frac{1}{\sqrt{2\pi s_{D,i}^2}} \exp \frac{-(g^i(\mathbf{m}) - d_{\text{obs}}^i)^2}{2s_{D,i}^2}, \quad (4)$$

where $g^i(\mathbf{m})$ is the i -th component of $g(\mathbf{m})$, d_{obs}^i is the observed value of the i -th component of \mathbf{d} , and $s_{D,i}$ is the standard deviation of the i -th observation (measurement uncertainty).

4.2.5 Calculation of the posterior probability distribution

The solution of the inverse problem is described by the posterior probability distribution $\sigma(\mathbf{d}, \mathbf{m})$:

$$\sigma(\mathbf{d}, \mathbf{m}) = k \rho_{\mathbf{M}}(\mathbf{m}) L(\mathbf{m}), \quad (5)$$

where k is a normalization constant.

We solve Eq. (5) by Monte Carlo Markov Chain (MCMC) to estimate the posterior probability distribution of a suite of model realizations. The MCMC method provides great flexibility at the cost of computational expense. For the current problem, the forward model is small and cheap (multiplication of a vector with a 10×10 matrix), so

the computational expense required to produce and analyze a large Monte Carlo ensemble is acceptable. While a full EMAC model run in the setup used for this study requires approximately 70 CPU hours of computation, the matrix multiplication can be performed one million times in less than 0.01 s of CPU time.

We consider the five sensitivity cases described in Table 3, particle sizes in 1 μm increments from 1 to 10 μm , and CCN-ACTIVE vs CCN-INACTIVE particles. For each combination of values of these parameters, we derive a separate inter-ecosystem transport matrix \mathbf{G} , for a total of 100 different cases. For each case, we performed a full atmospheric model simulation to generate a realization of \mathbf{G} , followed by an MCMC inversion with one million trials. The lowest acceptance rate was ca. 15 %, producing an ensemble with more than one-hundred-fifty-thousand members.

The ensemble generated is interpreted as an estimate of $\sigma(\mathbf{m})$. The center of the ensemble is interpreted as an estimate of \mathbf{m} , and the spread of the ensemble as an estimate of the uncertainty in \mathbf{m} . As a measure of the center, we use the mode (from the half range mode estimator of Bickel, 2002), as testing revealed that the mode gave a more robust indication of the location of the ensemble peak, particularly in the PRIOR-POS simulations (compare Fig. A3). As a measure of the ensemble spread, we use the 5–95 %-ile range.

4.3 Results of Monte Carlo inversion and discussion

4.3.1 Posterior probability distributions (ensembles)

The posterior distributions of the estimated fluxes for each particle size and source ecosystem are shown as histograms in Fig. A3 and Fig. A4. In each case, the typical posterior distribution of flux estimates for each ecosystem has an approximately Gaussian shape, which results from the assumption that the observation uncertainty has a Gaussian distribution.

In NO-PRIOR, negative (deposition) fluxes are allowed, and in some regions the most likely estimate of the flux is negative. Flux estimates in different regions are highly

Impact of particle characteristics on inferred emissions

S. M. Burrows et al.

Title Page

Abstract

Introduction

Conclusions

References

Tables

Figures



Back

Close

Full Screen / Esc

Printer-friendly Version

Interactive Discussion



cross-correlated, as increases in emissions in one region are compensated by decreases in other regions (Fig. A1).

In PRIOR-POS, the typical posterior distribution has the shape of a Gaussian distribution abruptly cut off at zero. This is because negative fluxes are disallowed, and the correlations between flux estimates in the different regions become very small: the additional constraint has the effect of somewhat decoupling the emissions from different regions (Fig. A2).

4.3.2 Global annual mass emissions and sensitivity to model parameters

Figure 2 shows the distribution of the global annual mass emitted for the MCMC ensemble, for PRIOR-POS (with a positive constraint on the emissions). Some apparent features are:

1. a right-skewed distribution of the ensembles, with more high extreme values than low extreme values: this results directly from the prior positive constraint on the emissions;
2. an increase in estimated emissions with increasing particle size, as shorter particle residence times require larger emissions to match the observed number concentrations;
3. higher estimated emissions for CCN-ACTIVE particles than for CCN-INACTIVE particles; again, shorter particle lifetimes require larger emissions to match the observed concentrations.

The uncertainties in global mean emissions contributed from cold and mixed-phase ice nucleation scavenging, CCN activity, particle size, observation uncertainty are shown in Fig. 3.

Impact of particle characteristics on inferred emissions

S. M. Burrows et al.

Title Page

Abstract

Introduction

Conclusions

References

Tables

Figures



Back

Close

Full Screen / Esc

Printer-friendly Version

Interactive Discussion



Sensitivity of global and regional emissions to particle size

As particle size increases, not only do estimated emissions increase globally, but estimated emissions for individual ecosystems typically increase as well. This can be seen, for example, in the histograms of the ecosystem emission estimates, especially when the emissions in each ecosystem are constrained to be positive (Fig. A3). When emissions are not constrained to be positive, this pattern is less clear (Fig. A4), especially for wetlands and coastal regions. These regions are poorly constrained by the observations due to their relatively small contribution to simulated concentrations: even large changes in the emissions in these regions have only a small influence on the concentrations in other regions, or on global emissions.

Comparison with previous work

The results of the MCMC estimation agree well with results from the constrained linear optimization for the same problem, as presented in Burrows et al. (2009a). In particular, the total uncertainty attributed to data uncertainty is reduced by nearly half. For 1 μm , CCN-ACTIVE tracers, the 5-%ile to 95-%ile range is 400–1800 Gga^{-1} in Burrows et al. (2009a), compared with 470–1100 Gga^{-1} from the MCMC ensemble, a reduction in the uncertainty range of 45%. The narrower range of the uncertainty in the present study may be due to the fact that we here treat the observation uncertainty as having a Gaussian probability distribution, rather than a homogeneous probability distribution. Also, the ecosystems shown in Burrows et al. (2009a) to be most poorly constrained by the observations, wetlands and coastal regions, were similarly poorly constrained when using the Monte Carlo method. This is apparent in the broad spread and irregular shapes of the distributions in those regions (Fig. 2).

ACPD

13, 4391–4432, 2013

Impact of particle characteristics on inferred emissions

S. M. Burrows et al.

Title Page

Abstract

Introduction

Conclusions

References

Tables

Figures

◀

▶

◀

▶

Back

Close

Full Screen / Esc

Printer-friendly Version

Interactive Discussion



5 Normalized model uncertainties

5.1 Definition and calculation of normalized model uncertainty

Comparing the uncertainties in the inversion that arise from the observation uncertainty with those that arise from model parameters (particle size, ice scavenging parameters and CCN activity) can assist in developing understanding of the relative utility of investing research efforts in various aspects of model development or in further observations.

To compare the effects of observation uncertainty and model parameter uncertainty, we quantify each individually and introduce a measure of “normalized model uncertainty” comparing the two. We quantify the effect of observation uncertainty on source estimates as the middle 90 % of the posterior distribution (“spread”). We quantify the linear sensitivity to continuous parameters (size and ice scavenging parameters) as the change in the center of the posterior distribution resulting from a small, finite change in the value of the parameter. Using these two quantities, we define the “linear model uncertainty” resulting from a given parameter, for continuous parameters (particle size and ice nucleation scavenging efficiency):

Linear model uncertainty =

$$\text{Difference in center of posterior distribution} \times \frac{\text{Parameter uncertainty}}{\text{Difference in parameter}} \quad (6)$$

and the “model uncertainty” for discontinuous parameters (CCN-ACTIVE vs. CCN-INACTIVE):

$$\text{Model uncertainty} = \text{Difference in center of posterior distribution.} \quad (7)$$

The parameter uncertainty ranges are listed in Table 4.

We further define the “normalized model uncertainty” as the contribution of model uncertainty to the uncertainty in the posterior distribution, normalized relative to the

Impact of particle characteristics on inferred emissions

S. M. Burrows et al.

Title Page

Abstract

Introduction

Conclusions

References

Tables

Figures

◀

▶

◀

▶

Back

Close

Full Screen / Esc

Printer-friendly Version

Interactive Discussion



observation uncertainty, i.e.:

$$\text{Normalized model uncertainty} = \frac{\text{(Linear) model uncertainty}}{\text{Mean spread in posterior distribution}}, \quad (8)$$

where the “spread” is given by the middle 90 % range in the respective posterior distribution, and the denominator is the average of the spreads in the two sensitivity cases.

The values used for the parameter uncertainty ranges and the observation uncertainty are summarized in Table 4.

The normalized model uncertainty allows us to summarize the uncertainties resulting from different model parameters and place them on a single, dimensionless scale. A normalized uncertainty near unity means that the contributions of the uncertainty in the model parameter and of the uncertainty in the observations are roughly equivalent. A normalized uncertainty much less than unity implies that the model uncertainty for this parameter is much smaller than the observation uncertainty, while a normalized uncertainty much greater than unity implies that the model uncertainty is much greater than the observation uncertainty for this parameter.

To calculate the normalized CCN uncertainty, we calculate the difference between the centers of the posterior distributions for each pair of CCN-ACTIVE and CCN-INACTIVE cases where all other factors are held constant (Eq. 7).

To calculate the normalized size uncertainty, we calculate the difference between the centers of each neighboring pair of particle sizes (i.e. 1 μm and 2 μm ; 2 μm and 3 μm , and so on), where all other factors are held constant (Eq. 6).

To calculate the cold and mixed ice scavenging uncertainties, we used the differences between the BASE case and the LIM_COLD and LIM_MIXED cases, respectively, where the ice nucleation scavenging coefficient is perturbed and all other factors are held constant (Eq. 6).

In each case, we then normalize the result by calculating the spread in each of the pair of distributions and then calculating the mean value of these spreads (Eq. 8).

Impact of particle characteristics on inferred emissions

S. M. Burrows et al.

Title Page

Abstract

Introduction

Conclusions

References

Tables

Figures



Back

Close

Full Screen / Esc

Printer-friendly Version

Interactive Discussion



5.2 Partitioning of uncertainty in total global emissions

Overall, the estimated total global mass emissions increase with increasing particle size. In parallel, the overall uncertainty in the global emissions increases in absolute terms but remains near 150 % of the median global flux estimate. The magnitude and sources of the estimated uncertainty are shown in Fig. 3. The uncertainty contribution from CCN activity seems to be fairly constant in absolute terms across the size range of interest, but decreases in relative terms for larger particles.

This is compensated by a growth in the uncertainty contribution from particle size, which increases both in relative and in absolute terms for larger particles. The contributions from ice scavenging parameters are comparatively small, although mixed-phase ice scavenging contributes more uncertainty than particle size for particle diameters from 1–4 μm .

5.3 Normalized model uncertainty results

The normalized model uncertainties in the estimated global mean emissions are compared in Fig. 4.

On average, the normalized model uncertainty from CCN activity is the largest. The additional effect of changing ice nucleation scavenging coefficients is minimal. The exception is the LIM_MIXED case, where normalized CCN uncertainty is reduced, at least for smaller particle sizes (Fig. 5, top; Fig. 6, bottom).

The normalized model uncertainty from particle size is slightly smaller than that from CCN activity. However, if the uncertainty in the particle size were appreciably larger than the $\pm 1 \mu\text{m}$ assumed here, then the particle size would be the largest contributor to the uncertainty in source estimation. Only a few measurements of the size of bacteria-carrying particles are available, but these suggest that at the locations studied, particles bearing culturable bacteria typically have diameters in the range of about 1–5 μm (e.g. Lighthart, 2000), so the uncertainty range in particle size could plausibly be as large as $\pm 2 \mu\text{m}$, rather than the $\pm 1 \mu\text{m}$ assumed in this study.

Title Page

Abstract

Introduction

Conclusions

References

Tables

Figures

◀

▶

◀

▶

Back

Close

Full Screen / Esc

Printer-friendly Version

Interactive Discussion



Impact of particle characteristics on inferred emissions

S. M. Burrows et al.

Title Page

Abstract

Introduction

Conclusions

References

Tables

Figures

⏪

⏩

◀

▶

Back

Close

Full Screen / Esc

Printer-friendly Version

Interactive Discussion



Figure 4 shows that the normalized model uncertainty for CCN activity is about 20 %–30 %. In Fig. 5, we show that the variability in this value is partly explained by the variation of CCN uncertainty with particle size. For 10 μm particles, the normalized model uncertainty for CCN activity is significantly smaller (close to 20 %) than for 1 μm particles (close to 40 %). This is attributable to the increasing ensemble spread (observation uncertainty) at larger particle sizes (Fig. 2), since the absolute magnitude of the CCN uncertainty remains roughly constant with varying particle size (Fig. 3).

Similarly, the normalized model uncertainty for particle size varies as a function of particle size. Model sensitivity to particle size is greater for larger particles and for CCN-INACTIVE particles. This is also seen in Fig. 1, where the steeper slopes of the lines indicates a higher sensitivity to particle size for larger particles, and for CCN-ACTIVE particles.

The statistical significance of each of these interactions between model parameters and the normalized model uncertainties is confirmed by a simple linear model, as illustrated in the linear effect diagrams shown in Fig. 6 (Fox, 1987, 2003).

The sensitivity to the CCN activity of the particles is high for particles of 1 μm diameter, decreasing to only moderate sensitivity for particles around 10 μm diameter (Fig. 5). The sensitivity to particle size is small to moderate for particles around 1 μm diameter, and increases to a large sensitivity for particles around 10 μm diameter. The sensitivity to particle size is higher for CCN-INACTIVE particles than for CCN-ACTIVE particles, particularly at particle sizes closer to 1 μm (Fig. 5).

6 Discussion and conclusions

For this case study, the observations consist of estimated characteristic annual mean concentrations of bacteria-containing particles for a set of ten ecosystems, as described in Burrows et al. (2009b). However, the methods described here for uncertainty estimation can be applied or adapted to a broad range of similar problems.

Impact of particle characteristics on inferred emissions

S. M. Burrows et al.

Title Page

Abstract

Introduction

Conclusions

References

Tables

Figures



Back

Close

Full Screen / Esc

Printer-friendly Version

Interactive Discussion



One aim of this study is to assess the extent to which the uncertainty in source inversions for aerosol transport is due to model parameter uncertainty as compared to observation uncertainty. The source inversion used as a case study here involves estimation of fluxes from highly uncertain concentration observations, and our previous work assumed that the model parameter uncertainties would be negligible relative to the observation uncertainties. However, our results suggest that even in this case study, with relatively large observation errors in concentration, model errors in particle size and scavenging characteristics can be significant. These sources of error should also be quantified and taken into account in source estimation for aerosol particles, either by estimating and including these modeling errors explicitly in the inversion, or by a post hoc analysis as presented here.

A Monte Carlo Markov Chain inversion was applied to estimate emissions of bacteria-containing particles from different ecosystems given a set of mean concentrations, analogous to Burrows et al. (2009a). The inversion produces results comparable to those obtained with a deterministic constrained linear optimization by Burrows et al. (2009a), with a reduction in the uncertainty range of 45 % for the global mean emissions estimate.

Uncertainty in the estimation of global mean emissions arises from both observation uncertainty and uncertainty in model parameters, including particle size, particle CCN activity, and the rate of ice nucleation scavenging in cold and mixed-phase clouds. Relative to the observation uncertainty (5 %ile to 95 %ile of the Monte Carlo ensemble), the normalized model uncertainty due to CCN activity or a change in particle size of 1 μm is typically between 10 % and 40 %. The model uncertainty from ice nucleation scavenging in cold clouds was negligible, but the normalized model uncertainty from ice nucleation scavenging in mixed-phase clouds was 10 %–20 %.

The sensitivity to scavenging in mixed-phase clouds is perhaps surprisingly large, a reflection of the large range of uncertainty in the process, for which it is difficult to find constraints from observations. Other studies have shown that simulated particle transport to high latitudes and the upper troposphere in particular is highly sensitive

to the scavenging rates in mixed-phase clouds, and moderately sensitive to scavenging rates in ice clouds (Burrows, 2011; Bourgeois and Bey, 2011; Zhang et al., 2012). As the relative contributions of different source regions to particulate air pollution in the Arctic has been a matter of significant interest for scientific research and public policy in recent years, this may deserve additional attention.

The contribution of model uncertainties in particle size and CCN activity was unexpectedly large compared to observation uncertainty for this case study, implying that these parameters should be better constrained by observations and/or the associated uncertainty should be explicitly considered in the inversion of atmospheric aerosol transport and uncertainty analyses in global atmospheric modelling studies involving aerosols. Ice nucleation scavenging in mixed-phase clouds in particular is rarely considered, but may contribute significantly to overall model uncertainty for problems involving aerosol transport. Even in cases with very large observation uncertainty, the contribution of model parameter uncertainty can be substantial.

Appendix A

Numerical approach

A1 Statistical model

Here we give a brief summary of the solution theory and method, closely following the presentation of Tarantola (2005).

We begin by defining the inverse problem as a combination of experimental, prior, and theoretical information, each of which can be represented as a probability density. We define several terms describing the problem:

1. the observable quantities d ,
2. the model (parameters) m ,

Impact of particle characteristics on inferred emissions

S. M. Burrows et al.

Title Page

Abstract

Introduction

Conclusions

References

Tables

Figures

◀

▶

◀

▶

Back

Close

Full Screen / Esc

Printer-friendly Version

Interactive Discussion



Impact of particle characteristics on inferred emissions

S. M. Burrows et al.

Title Page

Abstract

Introduction

Conclusions

References

Tables

Figures

◀

▶

◀

▶

Back

Close

Full Screen / Esc

Printer-friendly Version

Interactive Discussion



3. the model function $m \mapsto g(m)$. The model function is given by the product of the inter-ecosystem transfer matrix \mathbf{G} and the flux vector m :

$$g(m) = \mathbf{G}m. \quad (\text{A1})$$

4. The *prior probability density* $\rho(d, m)$ represents prior information constraining both the observable quantities and the model parameters.

If the data (observations of concentrations) are independent of the prior information about model parameters, we can write:

$$\rho(d, m) = \rho_D(d)\rho_M(m), \quad (\text{A2})$$

where $\rho_D(d)$ represents prior information about the observable quantities and $\rho_M(m)$ represents prior information about the model.

Here we assume that no information is available about the values of the observable parameters prior to the inversion, i.e. the measurements are the only source of information about the observable parameters:

$$\rho_D(d) = \mu_D(d). \quad (\text{A3})$$

For the prior information about the model, we treat two cases. In the case NO-PRIOR,

$$\rho_M(m) = \mu_M(m) \quad (\text{A4})$$

while in the case PRIOR-POS,

$$\rho_M(m) = \begin{cases} \mu_M(m), & m \geq 0 \\ 0, & m < 0 \end{cases}. \quad (\text{A5})$$

Impact of particle characteristics on inferred emissions

S. M. Burrows et al.

5. The *conditional probability* $\theta(\mathbf{d}|\mathbf{m})$ is the probability that the result of the model (the simulated data vector $\mathbf{G}\mathbf{m}$) is correct, given the data.

In this study, we assume that the observations are independent and their uncertainty is Gaussian-distributed. The discretized formulation of $\theta(\mathbf{d}|\mathbf{m})$ is then equal to the product of the normalized Gaussian probability density functions for each data point:

$$\theta(\mathbf{d}|\mathbf{m}) = \prod_{i=1}^N \frac{1}{\sqrt{2\pi s_{D,i}^2}} \exp \frac{-(g^i(\mathbf{m}) - \mathbf{d}_{\text{obs}}^i)^2}{2s_{D,i}^2}, \quad (\text{A6})$$

where $\mathbf{d}_{\text{obs}}^i$ is the observed value of the i -th component of \mathbf{d} , $s_{D,i}$ is the standard deviation of the i -th observation (measurement uncertainty), and $g^i(\mathbf{m})$ is the i -th component of $g(\mathbf{m})$,

$$g^i(\mathbf{m}) = \sum_{j=1}^M \mathbf{G}_{ij} m_j. \quad (\text{A7})$$

A2 Solution of the inverse problem

The solution of the inverse problem, the posterior probability distribution, $\sigma_M(\mathbf{d}, \mathbf{m})$, is given by:

$$\sigma_M(\mathbf{d}, \mathbf{m}) = k \rho_M(\mathbf{m}) L(\mathbf{m}), \quad (\text{A8})$$

where k is a normalization constant and $\rho_M(\mathbf{m})$ is the prior probability density in the model space. The likelihood function $L(\mathbf{m})$ is a measure of how well a candidate model \mathbf{m} explains the observations:

$$L(\mathbf{m}) = \int_{\text{ID}} d\mathbf{d} \frac{\rho_D(\mathbf{d}) \theta(\mathbf{d}|\mathbf{m})}{\mu_D(\mathbf{d})}, \quad (\text{A9})$$

Title Page

Abstract

Introduction

Conclusions

References

Tables

Figures

◀

▶

◀

▶

Back

Close

Full Screen / Esc

Printer-friendly Version

Interactive Discussion



where $\int_{\mathcal{D}}$ is the integral over the data space \mathcal{D} .

Using Eqs. (A3) and (A6), we can directly calculate the likelihood function:

$$L(\mathbf{m}) = \int_{\mathcal{D}} d\mathbf{d} \theta(\mathbf{d}|\mathbf{m}) = \prod_{i=1}^N \frac{1}{\sqrt{2\pi s_{D,i}^2}} \exp \frac{-(g^i(\mathbf{m}) - \mathbf{d}_{\text{obs}}^i)^2}{2s_{D,i}^2}, \quad (\text{A10})$$

A3 The Metropolis Algorithm

To solve the inversion problem, we apply a Monte Carlo Metropolis Chain algorithm (Metropolis et al., 1953), generating a large ensemble of solutions via a random walk algorithm, and applying a probabilistic rule to preferentially select solutions that have a higher likelihood.

1. Select initial guess for model parameters \mathbf{m}_0 .
2. Add a small random vector $\boldsymbol{\epsilon}$ to select next candidate solution,

$$\mathbf{m}_{i+1} = \mathbf{m}_i + \boldsymbol{\epsilon}. \quad (\text{A11})$$

3. Obtain a sample of the prior distribution: Apply the Metropolis rule to determine whether to accept or reject the candidate solution based on the prior probability density $\rho_{\text{M}}(\mathbf{m})$:

- (a) If $\rho_{\mathbf{m}_{i+1}} \geq \rho_{\mathbf{m}_i}$, accept the proposed transition to \mathbf{m}_{i+1} .
- (b) If $\rho_{\mathbf{m}_{i+1}} < \rho_{\mathbf{m}_i}$, then accept the proposed move with probability

$$P_{i \rightarrow i+1} = \frac{\rho_{\mathbf{m}_{i+1}}}{\rho_{\mathbf{m}_i}}. \quad (\text{A12})$$

For PRIOR-POS, all candidate solutions m_j in which all elements (individual model fluxes) are non-negative are retained, while all candidates with negative elements are rejected (Eq. A5). The retained m_j are a sample of the the prior ensemble.

4. For each member of the prior ensemble, calculate the likelihood function and apply the Metropolis rule to determine whether to accept or reject the candidate solution:

(a) If $L(\mathbf{m}_{i+1}) \geq L(\mathbf{m}_i)$, accept the proposed transition to \mathbf{m}_{i+1} .

(b) If $L(\mathbf{m}_{i+1}) < L(\mathbf{m}_i)$, then accept the proposed move with probability

$$P_{i \rightarrow j} = \frac{L(\mathbf{m}_{i+1})}{L(\mathbf{m}_i)}. \quad (\text{A13})$$

5. Repeat steps 2.–4. for the desired number of trials.

Given a sufficiently large number of iterations, the ensemble of models (candidate solutions) \mathbf{m}_i is a good approximation to a random sample of the posterior probability distribution $\sigma(\mathbf{d}, \mathbf{m})$, i.e. the solution to the inverse problem (Eq. A8; Metropolis et al., 1953; Mosegaard and Tarantola, 1995) The center and spread of the ensemble can be used to derive estimates of the solution and uncertainty.

Note that because only the ratios of the likelihoods associated with each model are of interest, there is no need to know the normalization parameter k , which remains constant.

Acknowledgements. Peter Rayner is in receipt of an Australian Professorial Fellowship (DP1096309). Susannah Burrows' work was partially funded by the the DOE Office of Science Biological and Environmental Research Program under their Earth System Modeling Program. The Pacific Northwest National Laboratory is operated for DOE by Battelle Memorial Institute under contract DE-AC06-76RLO 1830. We gratefully acknowledge the efforts of the EMAC development team to develop and make available the EMAC modelling system.

The service charges for this open access publication have been covered by the Max Planck Society.

Impact of particle characteristics on inferred emissions

S. M. Burrows et al.

Title Page

Abstract

Introduction

Conclusions

References

Tables

Figures



Back

Close

Full Screen / Esc

Printer-friendly Version

Interactive Discussion



References

- Bickel, D.: Robust estimators of the mode and skewness of continuous data, *Comput. Stat. Data An.*, 39, 153–163, 2002. 4403
- Bourgeois, Q. and Bey, I.: Pollution transport efficiency toward the Arctic: sensitivity to aerosol scavenging and source regions, *J. Geophys. Res.*, 116, D08213, 2011. 4411
- Burrows, S. M.: Sources and concentrations of biological particles in the global atmosphere, and their significance as ice nuclei, PhD thesis, Max Planck Graduate Center mit der Johannes Gutenberg-Universität, Mainz, 2011. 4411
- Burrows, S. M., Butler, T., Jöckel, P., Tost, H., Kerkweg, A., Pöschl, U., and Lawrence, M. G.: Bacteria in the global atmosphere – Part 2: Modeling of emissions and transport between different ecosystems, *Atmos. Chem. Phys.*, 9, 9281–9297, doi:10.5194/acp-9-9281-2009, 2009a. 4395, 4396, 4405, 4410, 4419, 4420
- Burrows, S. M., Elbert, W., Lawrence, M. G., and Pöschl, U.: Bacteria in the global atmosphere – Part 1: Review and synthesis of literature data for different ecosystems, *Atmos. Chem. Phys.*, 9, 9263–9280, doi:10.5194/acp-9-9263-2009, 2009b. 4395, 4409, 4419
- Després, V. R., Huffman, J. A., Burrows, S. M., Hoose, C., Safatov, A. S., Buryak, G., Fröhlich-Nowoisky, J., Elbert, W., Andreae, M. O., Pöschl, U., and Jaenicke, R.: Primary biological aerosols in the atmosphere: a review of observations and relevance, *Tellus B*, 64, 15598, doi:10.3402/tellusb.v64i0.15598, 2012. 4393
- Fox, J.: Effect displays for generalized linear models, *Sociol. Methodol.*, 17, 347–361, 1987. 4409
- Fox, J.: Effect displays in R for generalised linear models, *J. Stat. Softw.*, 8, 1–27, 2003. 4409
- Henning, S., Bojinski, S., Diehl, K., Ghan, S., Nyeki, S., Weingartner, E., Wurzler, S., and Baltensperger, U.: Aerosol partitioning in natural mixed-phase clouds, *Geophys. Res. Lett.*, 31, L06101, doi:10.1029/2003GL019025, 2004. 4398
- Huneeus, N., Schulz, M., Balkanski, Y., Griesfeller, J., Prospero, J., Kinne, S., Bauer, S., Boucher, O., Chin, M., Dentener, F., Diehl, T., Easter, R., Fillmore, D., Ghan, S., Ginoux, P., Grini, A., Horowitz, L., Koch, D., Krol, M. C., Landing, W., Liu, X., Mahowald, N., Miller, R., Morcrette, J.-J., Myhre, G., Penner, J., Perlwitz, J., Stier, P., Takemura, T., and Zender, C. S.: Global dust model intercomparison in AeroCom phase I, *Atmos. Chem. Phys.*, 11, 7781–7816, doi:10.5194/acp-11-7781-2011, 2011. 4393

Impact of particle characteristics on inferred emissions

S. M. Burrows et al.

Title Page

Abstract

Introduction

Conclusions

References

Tables

Figures

◀

▶

◀

▶

Back

Close

Full Screen / Esc

Printer-friendly Version

Interactive Discussion



- Jaenicke, R.: Abundance of cellular material and proteins in the atmosphere, *Science*, 308, p. 73, doi:10.1126/science.1106335, 2005. 4393
- Kerkweg, A., Buchholz, J., Ganzeveld, L., Pozzer, A., Tost, H., and Jöckel, P.: Technical Note: An implementation of the dry removal processes DRY DEPosition and SEDImentation in the Modular Earth Submodel System (MESSy), *Atmos. Chem. Phys.*, 6, 4617–4632, doi:10.5194/acp-6-4617-2006, 2006a. 4396
- Kerkweg, A., Sander, R., Tost, H., and Jöckel, P.: Technical note: Implementation of prescribed (OFFLEM), calculated (ONLEM), and pseudo-emissions (TNUDGE) of chemical species in the Modular Earth Submodel System (MESSy), *Atmos. Chem. Phys.*, 6, 3603–3609, doi:10.5194/acp-6-3603-2006, 2006b. 4396
- Kinne, S., Schulz, M., Textor, C., Guibert, S., Balkanski, Y., Bauer, S. E., Bernsten, T., Berglen, T. F., Boucher, O., Chin, M., Collins, W., Dentener, F., Diehl, T., Easter, R., Feichter, J., Fillmore, D., Ghan, S., Ginoux, P., Gong, S., Grini, A., Hendricks, J., Herzog, M., Horowitz, L., Isaksen, I., Iversen, T., Kirkevåg, A., Kloster, S., Koch, D., Kristjansson, J. E., Krol, M., Lauer, A., Lamarque, J. F., Lesins, G., Liu, X., Lohmann, U., Montanaro, V., Myhre, G., Penner, J., Pitari, G., Reddy, S., Seland, O., Stier, P., Takemura, T., and Tie, X.: An AeroCom initial assessment – optical properties in aerosol component modules of global models, *Atmos. Chem. Phys.*, 6, 1815–1834, doi:10.5194/acp-6-1815-2006, 2006. 4393
- Lawrence, M. and Rasch, P.: Tracer transport in deep convective updrafts: Plume ensemble versus bulk formulations, *J. Atmos. Sci.*, 62, 2880–2894, 2005. 4396
- Lelieveld, J., Kunkel, D., and Lawrence, M. G.: Global risk of radioactive fallout after major nuclear reactor accidents, *Atmos. Chem. Phys.*, 12, 4245–4258, doi:10.5194/acp-12-4245-2012, 2012. 4396
- Lighthart, B.: Mini-review of the concentration variations found in the al fresco atmospheric bacterial populations, *Aerobiologia*, 16, 7–16, 2000. 4408
- Metropolis, N., Rosenbluth, A., Rosenbluth, M., Teller, A., and Teller, E.: Equation of state calculations by fast computing machines, *J. Chem. Phys.*, 21, 1087, 1953. 4414, 4415
- Mosegaard, K. and Tarantola, A.: Monte Carlo sampling of solutions to inverse problems, *J. Geophys. Res.*, 100, 12–431, 1995. 4415
- Olson, J.: World ecosystems (WE1.4): Digital raster data on a 10 minute geographic 1080 (2160 grid square), Global Ecosystem Database, Version, 1, ftp://ftp.ngdc.noaa.gov/hazards/ftp_seg/Ecosystems/CEOS_Ecoregions/datasets/a05/owe.htm (last access: February 2013), 1992. 4396

Impact of particle characteristics on inferred emissions

S. M. Burrows et al.

[Title Page](#)[Abstract](#)[Introduction](#)[Conclusions](#)[References](#)[Tables](#)[Figures](#)[◀](#)[▶](#)[◀](#)[▶](#)[Back](#)[Close](#)[Full Screen / Esc](#)[Printer-friendly Version](#)[Interactive Discussion](#)

- Pruppacher, H. and Klett, J.: Microphysics of Clouds and Precipitation, Kluwer Academic Pub., Dordrecht, The Netherlands, 1997. 4397, 4398
- Schwarzenböck, A., Mertes, S., Heintzenberg, J., Wobrock, W., and Laj, P.: Impact of the Bergeron-Findeisen process on the release of aerosol particles during the evolution of cloud ice, *Atmos. Res.*, 58, 295–313, 2001. 4398
- Seinfeld, J. H. and Pandis, S. N.: Atmospheric Chemistry and Physics: From Air Pollution to Climate Change, John Wiley, New York, 2006. 4398
- Solomon, S., Qin, D., Manning, M., Chen, Z., Marquis, M., Avery, K. B., Tignor, M., and Miller, H. L. (Eds.): Contribution of Working Group I to the Fourth Assessment Report of the Intergovernmental Panel on Climate Change, Cambridge, United Kingdom and New York, NY, USA, 2007. 4393
- Tarantola, A.: Inverse Problem Theory and Methods for Model Parameter Estimation, Philadelphia, Society for Industrial and Applied Mathematics, 2005. 4400, 4401, 4402, 4411
- Tost, H., Jöckel, P., Kerkweg, A., Sander, R., and Lelieveld, J.: Technical note: A new comprehensive SCAVenging submodel for global atmospheric chemistry modelling, *Atmos. Chem. Phys.*, 6, 565–574, doi:10.5194/acp-6-565-2006, 2006. 4396
- Tost, H., Lawrence, M. G., Brühl, C., Jöckel, P., The GABRIEL Team, and The SCOUT-O3-DARWIN/ACTIVE Team: Uncertainties in atmospheric chemistry modelling due to convection parameterisations and subsequent scavenging, *Atmos. Chem. Phys.*, 10, 1931–1951, doi:10.5194/acp-10-1931-2010, 2010. 4396
- Verheggen, B., Cozic, J., Weingartner, E., Bower, K., Mertes, S., Connolly, P., Gallagher, M., Flynn, M., Choulaton, T., and Baltensperger, U.: Aerosol partitioning between the interstitial and the condensed phase in mixed-phase clouds, *J. Geophys. Res.*, 112, D23202, 2007. 4398
- Zhang, K., O'Donnell, D., Kazil, J., Stier, P., Kinne, S., Lohmann, U., Ferrachat, S., Croft, B., Quaas, J., Wan, H., Rast, S., and Feichter, J.: The global aerosol-climate model ECHAM-HAM, version 2: sensitivity to improvements in process representations, *Atmos. Chem. Phys.*, 12, 8911–8949, doi:10.5194/acp-12-8911-2012, 2012. 4411

Impact of particle characteristics on inferred emissions

S. M. Burrows et al.

Table 1. Estimates of total mean number concentration of bacteria-containing particles [m^{-3}] in near-surface air of various ecosystem types, reproduced with corrections from Burrows et al. (2009b,a).

Ecosystem	Low estimate ^b	Best estimate ^a	High estimate	Percent uncertainty
coastal ^c	2.3×10^4	7.6×10^4	1.3×10^5	300
crops ^c	4.1×10^4	1.1×10^5	1.7×10^5	81
deserts ^{d,e}	1.6×10^2	<i>(1×10^4)</i>	3.8×10^4	380
forests ^f	3.3×10^4	5.6×10^4	8.8×10^4	100
grasslands ^{c,g}	2.5×10^4	1.1×10^5	8.4×10^5	290
land ice ^{h,i}	<i>(1×10^1)</i>	<i>(5×10^3)</i>	1×10^4	200
seas ^{c,g,j}	1×10^1	1×10^4	8×10^4	800
shrubs ^{f,g}	1.2×10^4	3.5×10^5	8.4×10^5	240
tundra ^{g,k}	<i>(1×10^1)</i>	1.2×10^4	5.6×10^4	470
wetlands ^l	2×10^4	9×10^4	8×10^5	870

^a Additional values have been assumed for fields left blank by Burrows et al. (2009a); these are denoted by parentheses and italic font.

^b Percent uncertainties are calculated as $\text{best} = (\text{high} - \text{low}) \times 100$.

^c Harrison et al. (2005).

^d Lighthart and Shaffer (1994).

^e Assumed the same as best estimate for seas.

^f Shaffer and Lighthart (1997)

^g Tong and Lighthart (1999); Tilley et al. (2001).

^h Bauer et al. (2002).

ⁱ Estimated low value for seas taken as lower bound, average of high and low values taken as best estimate.

^j Griffin et al. (2006).

^k Estimated low value for seas taken as lower bound.

^l Assumed to be within bounds of estimates in coastal and grassland/crops regions.

Title Page

Abstract

Introduction

Conclusions

References

Tables

Figures

◀

▶

◀

▶

Back

Close

Full Screen / Esc

Printer-friendly Version

Interactive Discussion



Impact of particle characteristics on inferred emissions

S. M. Burrows et al.

Title Page

Abstract

Introduction

Conclusions

References

Tables

Figures

◀

▶

◀

▶

Back

Close

Full Screen / Esc

Printer-friendly Version

Interactive Discussion



Table 2. Removal processes included for CCN-ACTIVE and CCN-INACTIVE particle types. The “+” and “–” symbols indicate, respectively, that the process is turned on or turned off for simulated removal of these particles. (Table adapted from Burrows et al., 2009a).

	Sedimentation	Dry deposition	Impaction and interception scavenging	Cloud droplet nucleation	Uptake by diffusion	Ice-phase scavenging (impaction and nucleation)
CCN-ACTIVE	+	+	+	+	+	+
CCN-INACTIVE	+	+	+	–	+	+

Impact of particle characteristics on inferred emissions

S. M. Burrows et al.

Table 3. Ice nucleation scavenging ratio in the three sensitivity setups.

	$T > -35^{\circ}\text{C}$	$T \leq -35^{\circ}\text{C}$
BASE	0.1	0.05
SENS_COLD	0.1	0.0505
SENS_MIXED	0.101	0.05
LIM_COLD	0.1	0.1
LIM_MIXED	0.7	0.05

Title Page

Abstract

Introduction

Conclusions

References

Tables

Figures

◀

▶

◀

▶

Back

Close

Full Screen / Esc

Printer-friendly Version

Interactive Discussion



Impact of particle characteristics on inferred emissions

S. M. Burrows et al.

Table 4. Uncertainty ranges (used for calculation of model uncertainty, observation uncertainty, and normalized model uncertainty).

Source of uncertainty	Uncertainty range
Observations	5-%ile–95-%ile of ensemble
Particle diameter	$\pm 1 \mu\text{m}$
CCN activity	yes/no
Mixed-phase ice scavenging	0.1–0.7
Cold ice scavenging	0.0–0.1

[Title Page](#)
[Abstract](#)
[Introduction](#)
[Conclusions](#)
[References](#)
[Tables](#)
[Figures](#)
[◀](#)
[▶](#)
[◀](#)
[▶](#)
[Back](#)
[Close](#)
[Full Screen / Esc](#)
[Printer-friendly Version](#)
[Interactive Discussion](#)


Impact of particle characteristics on inferred emissions

S. M. Burrows et al.

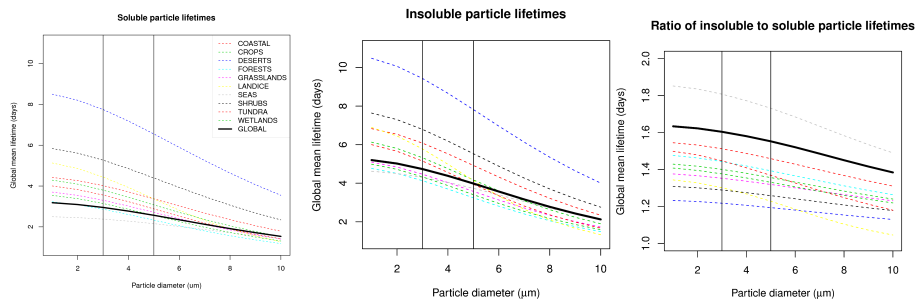


Fig. 1. Particle residence time in BASE model setup, as a function of particle aerodynamic diameter, emission ecosystem, and CCN activity. Left: CCN-ACTIVE, Middle: CCN-INACTIVE, Right: CCN-INACTIVE. The color key is indicated in the left panel.

Title Page

Abstract

Introduction

Conclusions

References

Tables

Figures

◀

▶

◀

▶

Back

Close

Full Screen / Esc

Printer-friendly Version

Interactive Discussion



Impact of particle characteristics on inferred emissions

S. M. Burrows et al.

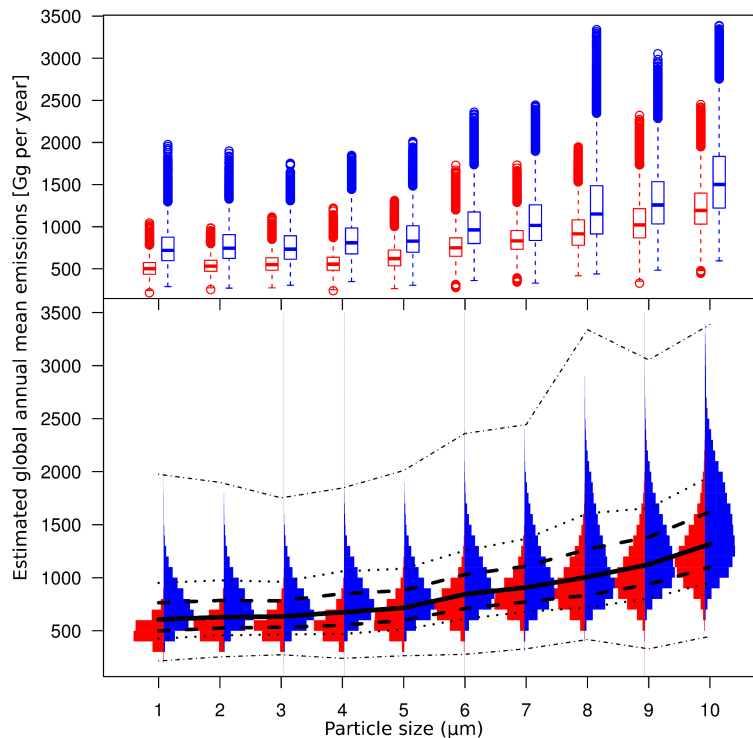


Fig. 2. Distributions of global annual mass emissions estimates [Gg per year] shown as boxplots (top) and histograms (bottom). Results are shown from left to right for each particle diameter from 1 μm to 10 μm , and for CCN-INACTIVE (red, on left for each size) and CCN-ACTIVE (blue, on right) particles. Lines in bottom panel demarcate the minimum, 10-%ile, 25-%ile, 50-%ile, 75-%ile, 90-%ile, and maximum of the total sample (CCN-ACTIVE and CCN-INACTIVE particles combined) for each particle size. Boxplots in top panel show distributions: thick lines show the median; box extent shows the 25-%ile to 75-%ile; whiskers extend up to 1.5 times the length of the box, or to the most extreme point; and dots show outliers beyond the whiskers. Results are for PRIOR-POS.

Title Page

Abstract

Introduction

Conclusions

References

Tables

Figures

◀

▶

◀

▶

Back

Close

Full Screen / Esc

Printer-friendly Version

Interactive Discussion



Impact of particle characteristics on inferred emissions

S. M. Burrows et al.

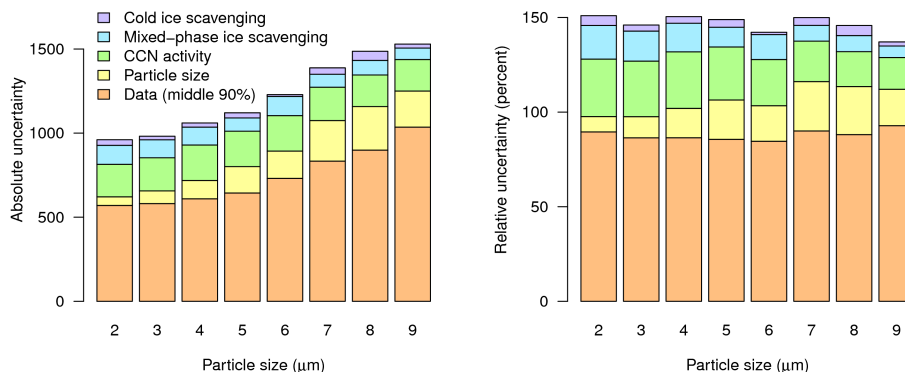


Fig. 3. Left: model and observation uncertainty in the inferred mean global flux (median per uncertainty type for various cases), expressed as absolute uncertainty. Right: Same, expressed as a relative uncertainty, i.e. (absolute uncertainty in global flux estimate)/(median global flux estimate) · 100. The sum of the individual uncertainties exceeds the value of the median global flux estimate in each case, resulting in relative uncertainties that exceed 100 %. The color key is indicated in the left panel.

Title Page

Abstract Introduction

Conclusions References

Tables Figures

◀ ▶

◀ ▶

Back Close

Full Screen / Esc

Printer-friendly Version

Interactive Discussion



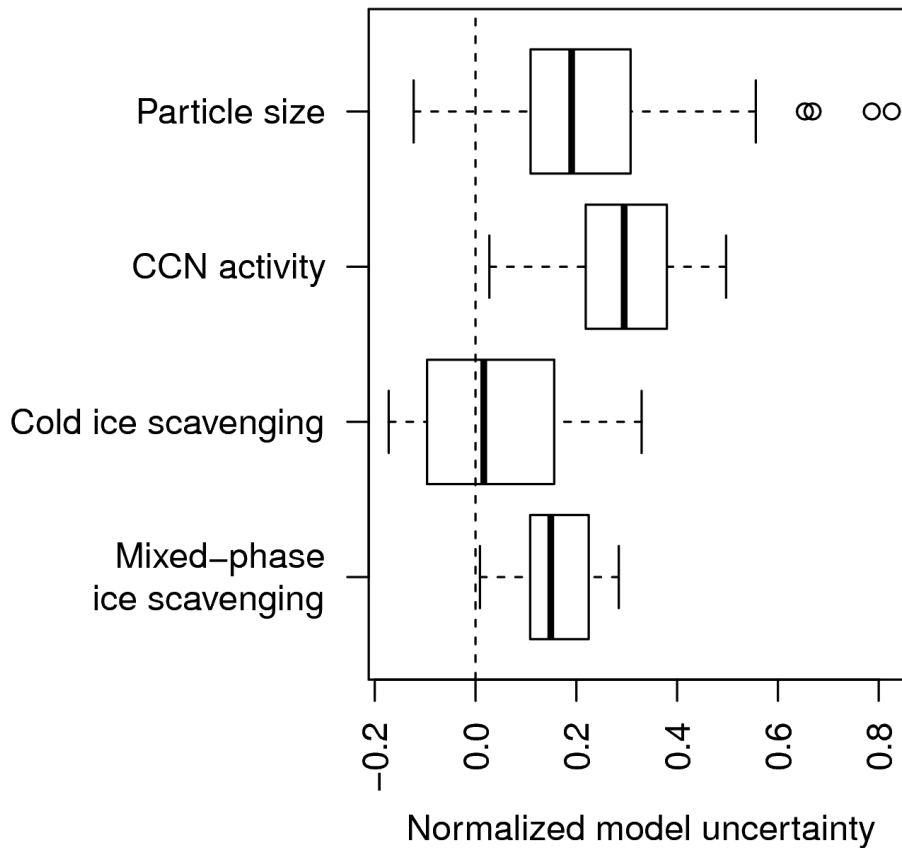


Fig. 4. Boxplot of the distributions of normalized model uncertainties for particle size, CCN activity, and the LIM_MIXED and LIM_COLD tests of the ice scavenging parameterization.

Impact of particle characteristics on inferred emissions

S. M. Burrows et al.

Title Page

Abstract

Introduction

Conclusions

References

Tables

Figures

◀

▶

◀

▶

Back

Close

Full Screen / Esc

Printer-friendly Version

Interactive Discussion



Impact of particle characteristics on inferred emissions

S. M. Burrows et al.

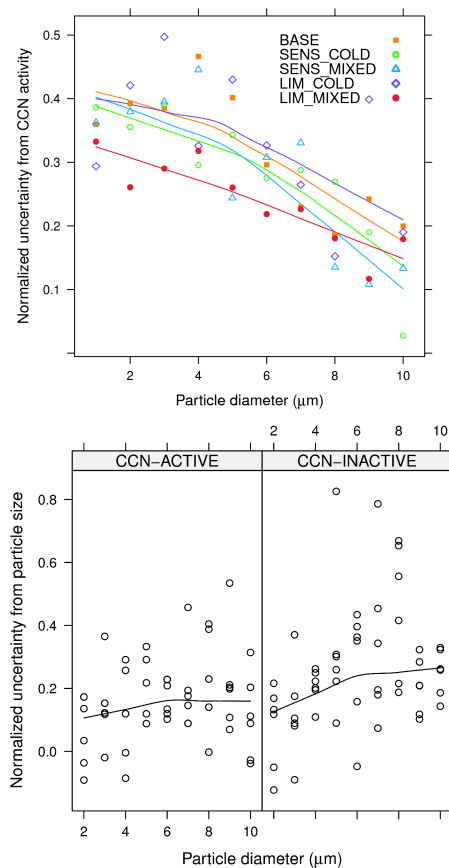


Fig. 5. Top: normalized model uncertainty from CCN activity, as a function of particle diameter. Bottom: normalized model uncertainty due to particle size, as a function of particle size. Lines in both panels are local polynomial regression fits to observations, and are provided as a guide to the eye. The color key is indicated in the top panel.

[Title Page](#)[Abstract](#)[Introduction](#)[Conclusions](#)[References](#)[Tables](#)[Figures](#)[◀](#)[▶](#)[◀](#)[▶](#)[Back](#)[Close](#)[Full Screen / Esc](#)[Printer-friendly Version](#)[Interactive Discussion](#)

Impact of particle characteristics on inferred emissions

S. M. Burrows et al.

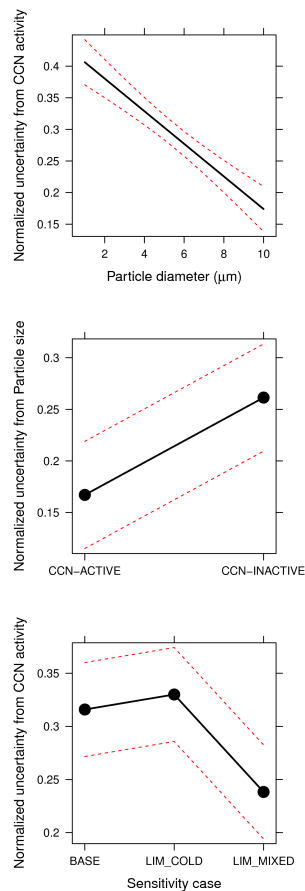


Fig. 6. Top: effect of particle size on CCN uncertainty. Middle: effect of CCN activity on size uncertainty. Bottom: effect of sensitivity case on CCN uncertainty. Red dashed lines indicate the 95 %-ile confidence interval.

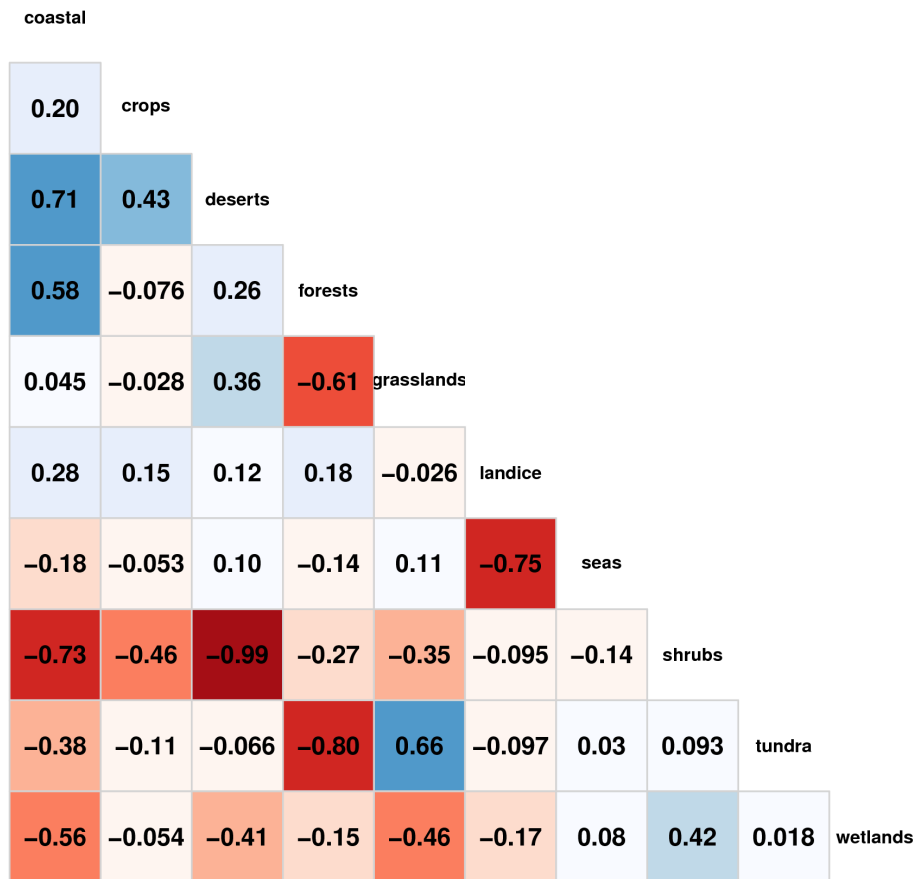


Fig. A1. Correlations between flux estimates for different ecosystems. Here for CCN-ACTIVE, 1 μm particles, in NO-PRIOR inversion (with no prior constraint on fluxes).

Impact of particle characteristics on inferred emissions

S. M. Burrows et al.

Title Page

Abstract Introduction

Conclusions References

Tables Figures

◀ ▶

◀ ▶

Back Close

Full Screen / Esc

Printer-friendly Version

Interactive Discussion



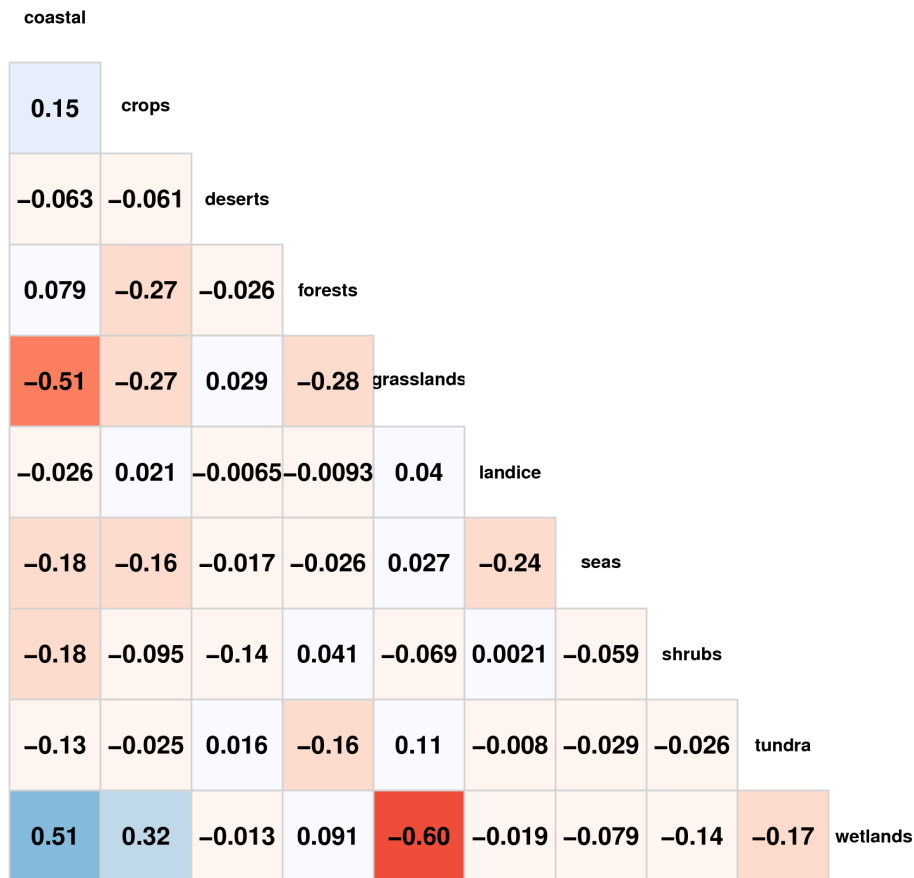


Fig. A2. Correlations between flux estimates for different ecosystems. Here for CCN-ACTIVE, 1 μm particles, in NO-PRIOR inversion (with prior positivity constraint on fluxes).

Impact of particle characteristics on inferred emissions

S. M. Burrows et al.

Title Page

Abstract Introduction

Conclusions References

Tables Figures

◀ ▶

◀ ▶

Back Close

Full Screen / Esc

Printer-friendly Version

Interactive Discussion



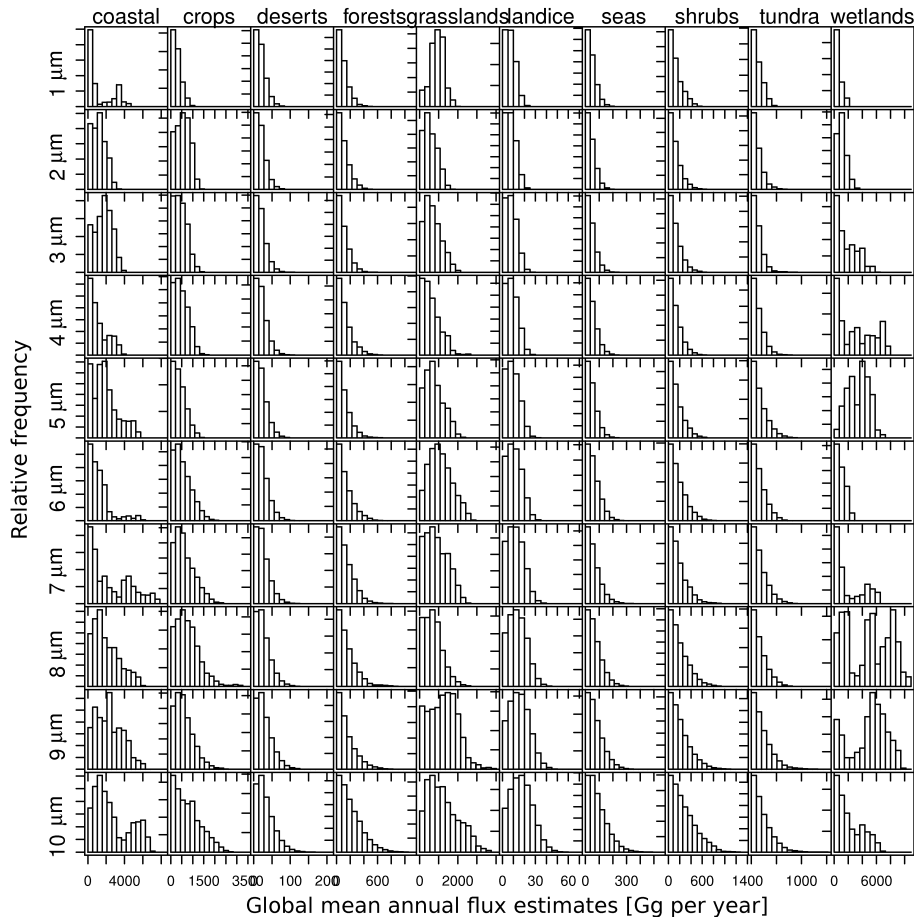


Fig. A3. Histograms of the Monte Carlo sample of flux estimates, for each ecosystem and particle sizes from 1 μm to 10 μm in 1 μm intervals. Here for CCN-ACTIVE particles in PRIOR-POS, with Gaussian data uncertainty and a prior positivity constraint on fluxes.

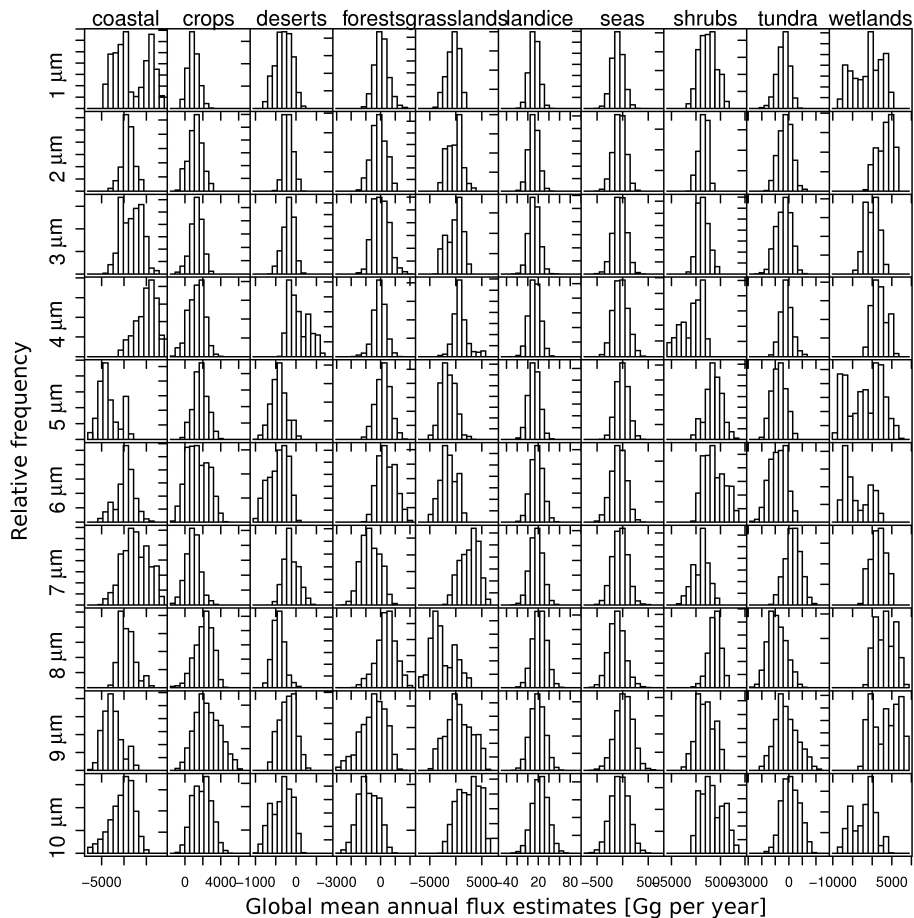


Fig. A4. Histograms of flux estimates, as in Fig. A3. Here for CCN-ACTIVE particles in NO-PRIOR, with Gaussian data uncertainty and no prior constraint on fluxes.